Internal stresses and textures of nanostructured alumina scales growing on polycrystalline Fe_3Al alloy

Pedro Brito[a)]
Institut für Angewandte Materialforschung, Helmholtz-Zentrum Berlin für Materialien und Energie, Albert-Einstein-Str. 15, Berlin 12489, Germany

Haroldo Pinto
Departamento de Engenharia de Materiais, Aeronáutica e Automobilística, Universidade de São Paulo, Av. Trabalhador São Carlense 400, São Carlos 13566-590, Brazil

Manuela Klaus, Christoph Genzel, and Anke Kaysser-Pyzalla
Institut für Angewandte Materialforschung, Helmholtz-Zentrum Berlin für Materialien und Energie, Albert-Einstein-Str. 15, Berlin 12489, Germany

(Received 19 March 2010; accepted 25 March 2010)

The evolution of internal stresses in oxide scales growing on polycrystalline Fe_3Al alloy in atmospheric air at 700 °C was determined using *in situ* energy-dispersive synchrotron X-ray diffraction. *Ex situ* texture analyses were performed after 5 h of oxidation at 700 °C. Under these conditions, the oxide-scale thickness, as determined by X-ray photoelectron spectroscopy, lies between 80 and 100 nm. The main phase present in the oxide scales is α-Al_2O_3, with minor quantities of metastable θ-Al_2O_3 detected in the first minutes of oxidation, as well as α-Fe_2O_3. α-Al_2O_3 grows with a weak (0001) fiber texture in the normal direction. During the initial stages of oxidation the scale develops, increasing levels of compressive stresses which later evolve to a steady state condition situated around −300 MPa. © *2010 International Centre for Diffraction Data.* [DOI: 10.1154/1.3402764]

Key words: oxidation, alumina, energy-dispersive diffraction, internal stress, texture

I. INTRODUCTION

Iron aluminides are considered as candidate materials for high-temperature applications due to their low cost, elevated strength to weight ratio, and excellent oxidation resistance. The oxidation resistance of these alloys relies upon the formation of a stable and protective α-Al_2O_3 scale that adheres to the metal surface and acts as a diffusion barrier for the underlying substrate against potentially hazardous corrosive environments (Prescott and Graham, 1992; Grabke, 1999). The important factors that affect the integrity of the protective oxide scale are growth stresses that develop within the scale, intrinsic to the oxidation process, and also the residual stresses that result after cooling to room temperature from the differences in thermal expansion between the metal substrate and the oxide (Tolpygo and Clarke, 1999). For this reason, much effort has been put forth in the past years to characterize the evolution of growth stresses in oxide scales during oxidation (Schumann *et al.*, 2000; Messaoudi *et al.*, 2000; Mennicke *et al.*, 2001; Clarke, 2002; Eschler *et al.*, 2004; Huntz *et al.*, 2007). In the specific case of Al_2O_3 forming alloys, recent studies have focused on the *in situ* determination of growth stresses during high-temperature oxidation (above 1000 °C) of Ni-Al and Fe-Cr-Al alloys using synchrotron radiation (Specht *et al.*, 2004; Veal *et al.*, 2006; Reddy *et al.*, 2007; Veal and Paulikas, 2008). However, in spite of these successful attempts to determine internal stresses in growing oxide scales, the mechanisms of strain formation during oxide growth are manifold (Evans, 1995) and not fully understood for a number of metal-oxide systems (Veal *et al.*, 2006; Clarke, 2003; Panicaud *et al.*, 2006).

Another important issue that affects the oxidation resistance of iron aluminides is the appearance of less protective Al_2O_3 polymorphs, generally monoclinic θ-Al_2O_3 or cubic γ-Al_2O_3, which only later transform into the stable α-Al_2O_3. These phases are formed when iron aluminides are subjected to low oxidation temperatures (below 1000 °C) and have a detrimental impact on the oxidation resistance of the alloy (Grabke, 1999; Levin and Brandon, 1998). The development of transition Al_2O_3 may also modify the stress state in the oxide layer since the transformation to α-Al_2O_3 is accompanied by a volume contraction (Rybicki and Smialek, 1989) which can induce tensile stresses into the first formed α-Al_2O_3 grains. Nevertheless, the evolution of phase composition in thermally growing alumina scales, especially in the early oxidation stages of Fe-Al alloys, remains yet to be clarified (Pöter *et al.*, 2005).

In order to further enhance the understanding on the mechanisms of internal strain formation during oxidation, the present work aims at the study of the microstructure (in terms of chemical composition, phase development, and crystallographic texture) and the stress evolution in oxide scales forming in atmospheric air on an intermetallic Fe–26 at. % Al alloy. A low oxidation temperature (700 °C) was applied in an attempt to favor the formation of metastable Al_2O_3 polymorphs.

II. EXPERIMENTAL

The specimens used in the oxidation experiments were 8-mm-diameter disks of 1 mm thickness cut from a polycrys-

a)Author to whom correspondence should be addressed. Electronic mail: ppbrito@gmail.com

talline Fe_3Al binary alloy ingot (Fe–26 at. % Al). The as-cast samples had grain sizes of a few hundred μm. Prior to oxidation, the samples were mechanically ground and polished to a 1 μm finish and thoroughly cleaned in ethanol. All oxidation experiments were performed at 700 °C in atmospheric air at ambient pressure.

The chemical composition in the oxide scales grown on Fe–26 at. % Al after 300 min was characterized by applying X-ray photoelectron spectroscopy (XPS). XPS spectra and sputter depth profiles were taken using a monochromatic Al $K\alpha$ X-ray source, step size of 0.8 eV, pass energy of 93.90 eV, 20 sweeps, and a spot size of 100 μm. The spectra were recorded within the binding energy range of 0 to 1200 eV, sputter depth profiles of the Fe 2*p*, Al 2*p*, and O 1*s* photolines were measured, and sputtering was performed with 2 keV Ar^+ ions in steps of approximately 10 nm (calibrated according to a SiO_2 standard). The XPS data were analyzed using the CASA-XPS software.

In order to assess the conditions for the appearance of metastable Al_2O_3 polymorphs, *ex situ* phase analyses applying grazing-incidence X-ray diffraction (XRD) at an incidence angle (ω) of 1° were carried out using a laboratory Co $K\alpha$ source for samples produced after different oxidation times, ranging from 2 to 300 min at 700 °C. Under these conditions, the penetration depth is estimated to be approximately 400 nm.

In situ oxidation experiments for stress analyses were carried out at the beamline for energy-dispersive diffraction (EDDI) of the Helmholtz-Zentrum Berlin, situated at the Berlin synchrotron radiation facility Berliner Elektronenspeicherring-Gesellschaft für Synchrotronstrahlung. The samples were oxidized in atmospheric air using an air-cooled resistance furnace. The time required to reach the desired oxidation temperature of 700 °C was approximately 10 min. The ED diffraction technique was applied (Genzel *et al.*, 2007) within an energy range of 15 to 85 keV and the internal stresses in the growing oxide scale were determined using the $\sin^2\psi$ method. In contrast to time-consuming angle-dispersive diffraction with monochromatic radiation, ED diffraction uses a polychromatic X-ray beam, thus allowing for the acquisition of complete ED diffractograms at a fixed 2θ angle. This enables the determination of stress values for several diffraction lines simultaneously (Juricic *et al.*, 2010).

In the present work the 2θ angle was set to 5°. The acquisition time for an individual ED diffractogram amounted to 5 min. The $\sin^2\psi$ measurements were performed using seven ψ tilts which resulted in a total measurement time, including sample movements, of 36 min/stress analysis. An *ex situ* texture analysis was also performed at the EDDI beamline on an Fe–26 at. % Al sample previously oxidized for 300 min at 700 °C. Pole-figure data were recorded for a ψ range of 0° to 75° in 5° steps and for an azimuthal φ range of 0° to 345° in 15° steps. Corrections of the pole-figure intensities were performed for absorption and geometrical aberrations (Welzel and Leoni, 2002) by measuring a randomly oriented W powder sample deposited on the oxidized sample. Complete pole figures and inverse pole figures were computed using the BEARTEX software, version 3.4 (Wenk *et al.*, 1998).

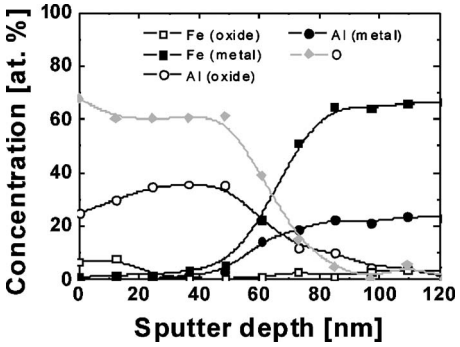

Figure 1. XPS sputter depth profile in the oxide scale grown on Fe–26 at. % Al substrate at 700 °C after 5 h oxidation time

III. RESULTS AND DISCUSSION

The chemical composition gradient in the scale grown on Fe–26 at. % Al after 5 h oxidation at 700 °C is presented in Fig. 1 (sputter depth values increase in the direction of the substrate). Scale thickness ranges between 80 and 100 nm and the scale appears to be formed exclusively by Al oxides except for a small concentration (lower than 10%) of Fe oxides which is restricted to the first 30 nm at the oxide outer surface. It is worth noticing that the concentration of Al^{+3} in the oxide scale, approximately 35%, is well above the nominal Al content in the base material (26%). This is an indication that oxide-scale growth occurs by outward diffusion of Al^{+3} cations as well as by the inward diffusion of O^{-2}, as it has been previously reported for the oxidation of other binary iron aluminides (Pöter *et al.*, 2005).

Phase analyses by grazing-incidence XRD were performed on samples oxidized for 2, 5, 10, 30, and 300 min at 700 °C. The diffraction data obtained for oxidation times of 5, 10, and 30 min are shown in Figs. 2(a)–2(c), respectively. The clear (220) diffraction line of the substrate, which appears in some of the samples, results from the coarse-grained substrates, which were prepared from different cast ingots. In spite of the low oxidation temperature applied, the XRD data show that even at the onset of the oxidation process α-Al_2O_3 is the predominant oxide phase in the scale, with only minor quantities of α-Fe_2O_3 and metastable θ-Al_2O_3. θ-Al_2O_3 appears to vanish already after 30 min of oxidation even though the development of the stable α-Al_2O_3 is usually associated with oxidation temperatures of over 1000 °C (Levin and Brandon, 1998; Pöter *et al.*, 2005). However, it has been noted that other oxides with trigonal crystal lattices, such as α-Fe_2O_3 and α-Cr_2O_3, may form at earlier stages and act as templates for the growth of α-Al_2O_3, thus favoring the earlier development of stable corundum at lower temperatures (Renusch *et al.*, 1997; Asteman and Spiegel, 2008). The results suggest, therefore, that the formation of α-Al_2O_3 occurs not only by transformation from θ-Al_2O_3 but also spontaneously as a consequence of the presence of α-Fe_2O_3 in the oxide scale.

Experimental pole figures were determined for the (104), (110), (113), and (116) diffraction lines of the α-Al_2O_3 developed after 5 h oxidation at 700 °C. These data were used for calculating the orientation distribution function (ODF) and inverse pole figures. Owing to the lower volume fraction of α-Fe_2O_3 in the oxide scale, the only pole figure that could be measured for this phase was the one corresponding to the

https://doi.org/10.1154/1.3402764 Published online by Cambridge University Press

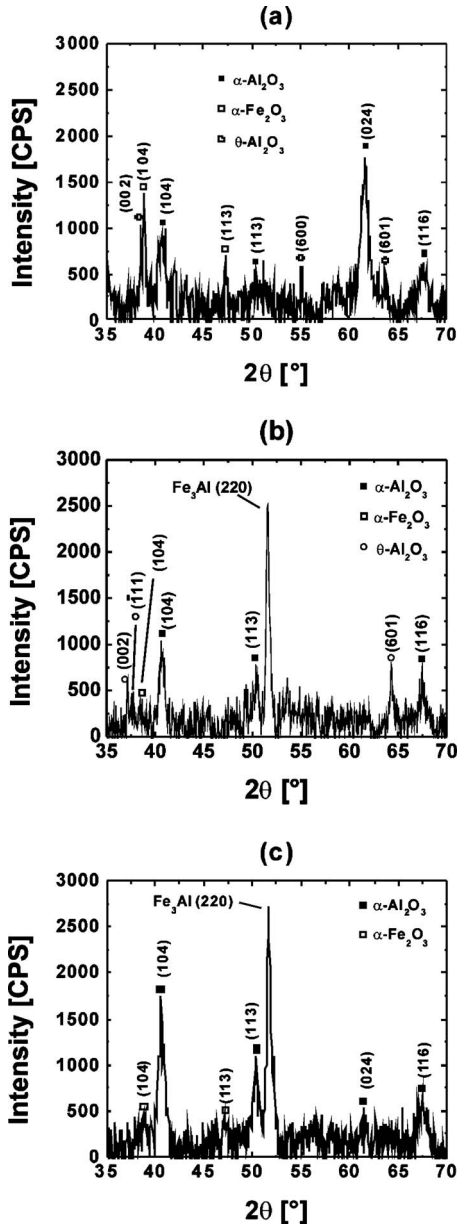

Figure 2. Grazing-incidence XRD patterns showing the oxide phases developed on Fe–26 at. % Al after (a) 5, (b) 10, and (c) 30 min of oxidation.

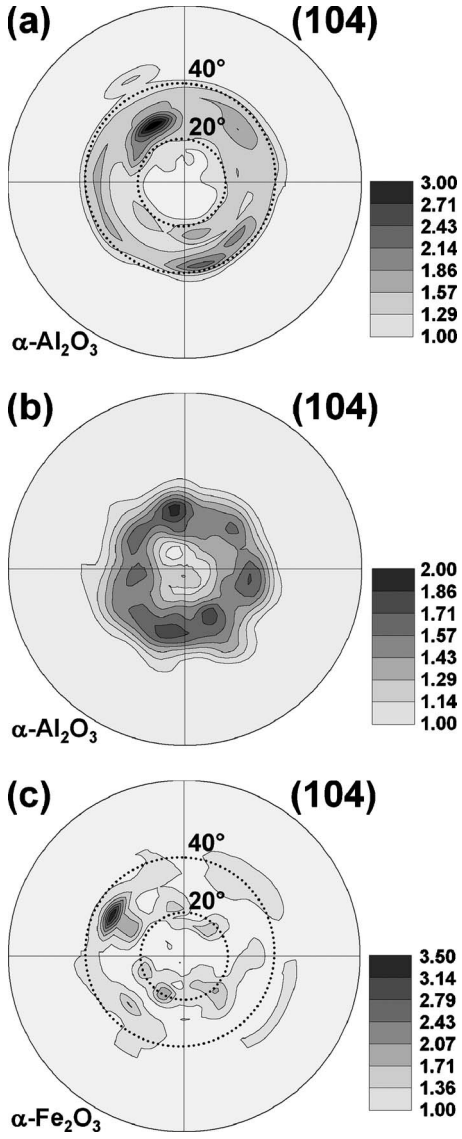

Figure 3. (a) Experimental (104) pole figure of α-Al_2O_3, (b) recalculated (104) pole figure of α-Al_3O_3, and (c) experimental (104) pole figure of α-Fe_2O_3 after 5 h oxidation of a Fe–26 at. % Al polycrystal at 700 °C. Texture strength is given in terms of mrd.

(104) reflection, which represents the strongest diffraction line. For this reason, it was not possible to determine the ODF or inverse pole figures for α-Fe_2O_3.

The experimental pole figure measured for the (104) diffraction line of α-Al_2O_3 is presented in Fig. 3(a). The corresponding recalculated pole figure obtained from the ODF is shown in Fig. 3(b). Figure 3(c) displays the experimental pole figure measured for the (104) diffraction line of α-Fe_2O_3. The texture strength is given in terms of multiples of a random distribution (mrd). The α-Fe_2O_3 pole figure is similar to the one of α-Al_2O_3 in the sense that in both cases the maximum texture strength occurs between polar distances of 20° to 40°. This suggests that the texture formation of both oxides is equivalent and could be a consequence of α-Fe_2O_3 acting as a crystallographic template for the formation of α-Al_2O_3. This observation is in agreement with studies of the epitaxy relation between α-Fe_2O_3 films grown on α-Al_2O_3, which show that the (0001) surfaces of both phases remain parallel to each other (Wang *et al.*, 2002; Lee *et al.*, 2005). Furthermore, Sun *et al.* (2006) suggested that the (0001) plane of another trigonal structured oxide, α-Cr_2O_3, provides favorable conditions for the template growth of α-Al_2O_3. Eklund *et al.* (2008), while observing that this template effect is stronger for α-Al_2O_3 developing on the (10-14) of α-Cr_2O_3, also reported the growth of textured (0001) α-Al_2O_3 on α-Cr_2O_3 (0001).

The inverse pole figure of α-Al_2O_3 in the normal direction (ND) of the scale surface is plotted in Fig. 4. It can be noticed that the (0001) basal planes of the corundum structure grow with a certain preferential orientation parallel to the surface of the sample. These results are in agreement with a previous electron backscattered diffraction study which also revealed a (0001) fiber texture in the ND of thermally grown α-Al_2O_3 scales (Karadge *et al.*, 2006). The texture strength of the oxide scale is, however, weak, thus allowing, e.g., for unrestricted $\sin^2\psi$ measurements. This

https://doi.org/10.1154/1.3402764 Published online by Cambridge University Press

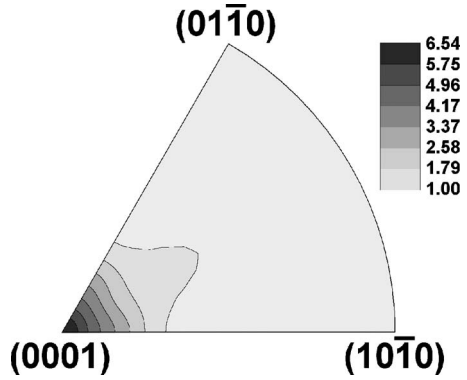

Figure 4. ND inverse pole figure of the α-Al_2O_3 grown on Fe–26 at. % Al after 5 h oxidation at 700 °C. Texture strength is given in terms of mrd.

agrees with the predictions of Blachère *et al.* (2003) that the ion mobility inside an oxide is low for oxidation temperatures below $T_m/2$ (T_m is the melting point of the oxide, here 2054 °C for α-Al_2O_3), causing a competitive oxide grain growth in the direction of the ion flux, i.e., parallel to the direction of the surface normal. This produces oxide scales which consist of stacks of α-Al_2O_3 grains without a strong crystallographic preferred orientation.

Figure 5 shows the evolution of the internal stresses in the oxide scale growing on Fe–26 at. % Al. The stresses were determined for the (012) and (104) diffraction lines. From the first stress analysis performed, at 45 min, to approximately 200 min of oxidation, the scale undergoes a continuous increase in the level of compressive stresses until a maximum average value of -630 ± 200 MPa [-720 ± 70 MPa, as determined for the (012) reflection, and -550 ± 200 MPa, as determined for the (104) reflection] is reached. The occurrence of compressive growth stresses during oxidation is attributed to the lateral growth mechanism of the oxide scale (Clarke, 2003; Rhines and Wolf, 1970). According to this model, Al^{+3} and O^{-2} diffusing in opposite directions combine to form new oxide grains along grain boundaries of the scale, which are oriented vertically to the surface. Since this new oxide is laterally constrained by the surrounding oxide grains as well as by the underlying substrate, high compressive stresses develop. After a maximum compressive stress level is reached in the scale, creep-induced stress relief begins to balance the intrinsic oxide growth stresses (Veal and Paulikas, 2008; Panicaud *et al.*, 2006; Limarga *et al.*, 2004), and the stress level in the oxide scale approaches a steady state condition which, in the present case, is close to −300 MPa.

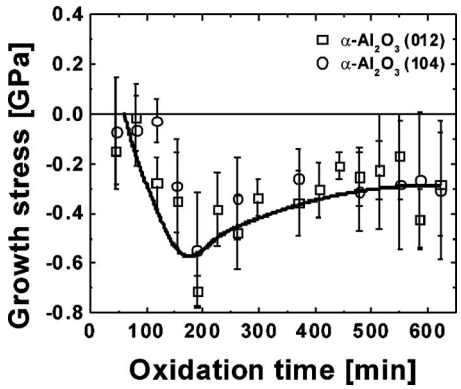

Figure 5. Evolution of growth stresses, determined for the (012) and (104) diffraction lines of α-Al_2O_3, with increasing oxidation times at 700 °C.

The strain evolution during the first 45 min of oxidation could not be characterized because of the long measurement times, which were necessary given the reduced thickness of these oxide scales. Thus, the impact of the appearance of θ-Al_2O_3 on the growth stress level could not be directly verified. However, the results obtained here appear to be consistent with previous studies (Veal and Paulikas, 2008; Hou *et al.*, 2007) in which it was observed that the first formed α-Al_2O_3 grains are under tensile stresses due to the development of metastable θ-Al_2O_3 and subsequent transformation of θ-Al_2O_3 to α-Al_2O_3. The extrapolation of the initial stress values (represented by the dotted line in Fig. 5) suggests the possibility of tensile stress formation during the first minutes of oxidation since it is rather unlikely that the oxide scale grows initially nearly stress-free, as the first determined stress values, ranging between -10 ± 100 and -70 ± 100 MPa, show. As displayed in Fig. 1(c), the θ-α transformation is completed before 30 min of oxidation time. After the metastable θ-Al_2O_3 is consumed, the compressive stress generation mechanism via new oxide growth inside the scale becomes predominant and the internal stresses change from tensile to compressive. The absence of tensile stresses in the scale during the later stages of oxidation further corroborates that metastable Al_2O_3 formation on the binary Fe–26 at. % Al alloy is restricted to the beginning of the oxidation process.

IV. CONCLUSION

The oxidation behavior of polycrystalline Fe_3Al in atmospheric air at 700 °C was studied. At this temperature, an oxide scale of approximately 80 to 100 nm forms on the metal surface. The scale is composed mostly of α-Al_2O_3 with minor quantities α-Fe_2O_3. A small amount of θ-Al_2O_3 was also shown to be present in the first minutes of oxidation. Texture analyses of the oxide scales formed after 5 h oxidation show that α-Al_2O_3 grows with a weak preferential orientation of the (0001) basal planes parallel to the oxidizing surface. It is also suggested that the similarities in texture between α-Fe_2O_3 and α-Al_2O_3 reflect the template effect of α-Fe_2O_3 for the nucleation of α-Al_2O_3 at lower temperatures. *In situ* stress analyses using ED synchrotron XRD showed that compressive stresses build up in the oxide scale after 45 min of oxidation as a result of new oxide growth inside the scale. In the first minutes, it is believed that the stress state is governed by the transformation of metastable θ-Al_2O_3 to α-Al_2O_3.

Asteman, H. and Spiegel, M. (**2008**). "A comparison of the oxidation behaviours of Al_2O_3 formers and Cr_2O_3 formers at 700 °C—Oxide solid solutions acting as a template for nucleation," Corros. Sci. **50**, 1734–1743.

Blachère, J. R., Schumann, E., Meier, G. H., and Pettit, F. S. (**2003**). "Texture of alumina scales on FeCrAl alloys," Scr. Mater. **49**, 909–912.

Clarke, D. R. (**2002**). "Stress generation during high-temperature oxidation of metallic alloys," Curr. Opin. Solid State Mater. Sci. **6**, 237–244.

Clarke, D. R. (**2003**). "The lateral growth strain accompanying the formation of thermally grown oxide," Acta Mater. **51**, 1393–1407.

Eklund, P., Sridharan, M., Sillassen, M., and Bøttiger, J. (**2008**). "α-Cr_2O_3

https://doi.org/10.1154/1.3402764 Published online by Cambridge University Press

texture template effect on α-Al_2O_3 thin-film growth," Thin Solid Films **516**, 7447–7450.
Eschler, H., Martinez, E. A., and Singheiser, L. (**2004**). "Residual stresses in alumina scales grown on different types of Fe-Cr-Al alloys: Effect of specimen geometry and cooling rate," Mater. Sci. Eng., A **384**, 1–11.
Evans, H. E. (**1995**). "Stress effects in high temperature oxidation of metals," Int. Mater. Rev. **40**, 1–40.
Genzel, Ch., Denks, I. A., Gibmeier, J., Klaus, M., and Wagener, G. (**2007**). "The materials science synchrotron beamline EDDI for energy-dispersive diffraction analysis," Nucl. Instrum. Methods Phys. Res. A **578**, 23–33.
Grabke, H. J. (**1999**). "The oxidation of NiAl and FeAl," Intermetallics **7**, 1153–1158.
Hou, P. Y., Paulikas, A. P., Veal, B. W., and Smialek, J. L. (**2007**). "Thermally grown Al_2O_3 on H_2-annealed Fe_3Al alloy: Stress evolution and film adhesion," Acta Mater. **55**, 5601–5613.
Huntz, A. M., Hou, P. Y., and Molins, R. (**2007**). "Study by deflection of the oxygen pressure influence on the phase transformation in alumina thin films formed by oxidation of Fe_3Al ," Mater. Sci. Eng., A **467**, 59–70.
Juricic, C., Pinto, H., Cardinali, D., Klaus, M., Genzel, Ch., and Pyzalla, A. R. (**2010**). "Effect of substrate grain size on the growth, texture and internal stresses of iron oxide scales forming at 450 °C ," Oxid. Met. **73**, 15–41.
Karadge, M., Zhao, Y., Preuss, M., and Xiao, P. (**2006**). "Microtexture of thermally grown alumina in commercial thermal barrier coatings," Scr. Mater. **54**, 639–644.
Lee, I. J., Kim, J.-Y., Yu, C., Chang, C.-H., Joo, M.-K., Lee, Y. P., Hur, T.-B., and Kim, H.-K. (**2005**). "Morphological and structural characterization of epitaxial α-Fe_2O_3 (0001) deposited on α-Al_2O_3 (0001) by dc sputter deposition," J. Vac. Sci. Technol. A **23**, 1450–1455.
Levin, I. and Brandon, D. (**1998**). "Metastable alumina polymorphs: Crystal structures and transition sequences," J. Am. Ceram. Soc. **81**, 1995–2012.
Limarga, A. M., Wilkinson, D. S., and Weatherly, G. C. (**2004**). "Modeling of oxidation-induced growth stresses," Scr. Mater. **50**, 1475–1479.
Mennicke, C., Clarke, D. R., and Rühle, M. (**2001**). "Stress relaxation in thermally grown alumina scales on heating and cooling FeCrAl and FeCrAlY alloys," Oxid. Met. **55**, 551–569.
Messaoudi, K., Huntz, A. M., and Di Menza, L. (**2000**). "Residual stress in alumina scales: Experiments, modeling, and stress-relaxation phenomena," Oxid. Met. **53**, 49–75.
Panicaud, B., Grosseau-Poussard, J. L., and Dinhut, J. F. (**2006**). "On the growth strain origin and stress evolution prediction during oxidation of metals," Appl. Surf. Sci. **252**, 5700–5713.
Pöter, B., Stein, F., Wirth, R., and Spiegel, M. (**2005**). "Early Stages of protective oxide layer growth on binary iron aluminides," Z. Phys. Chem. **219**, 1489–1503.
Prescott, R. and Graham, M. J. (**1992**). "The oxidation of iron aluminum alloys," Oxid. Met. **38**, 73–87.
Reddy, A., Hovis, D. B., Heuer, A., Paulikas, A. P., and Veal, B. W. (**2007**). "*In-situ* study of oxidation-induced growth strains in a model NiCrAlY bond-coat alloy," Oxid. Met. **67**, 153–177.
Renusch, D., Grimsditch, M., Koshelev, I., Veal, B. W., and Hou, P. Y. (**1997**). "Strain determination in thermally-grown alumina scales using fluorescence spectroscopy," Oxid. Met. **48**, 471–495.
Rhines, F. N. and Wolf, J. S. (**1970**). "The role of oxide microstructure and growth stresses in the high temperature scaling of nickel," Metall. Trans. **1**, 1701–1710.
Rybicki, G. C. and Smialek, J. L. (**1989**). "Effect of θ-α-Al_2O_3 transformation on the oxidation behavior of β-NiAl+Zr ," Oxid. Met. **31**, 275–304.
Schumann, E., Sarioglu, C., Blachere, J. R., Pettit, F. S., and Meier, G. H. (**2000**). "High-temperature stress measurements during the oxidation of NiAl," Oxid. Met. **53**, 259–272.
Specht, E. D., Tortorelli, P. F., and Zschack, P. (**2004**). "*In situ* measurement of growth stress in alumina scale," Powder Diffr. **19**, 69–73.
Sun, J., Stirner, T., and Matthews, A. (**2006**). "Structure and surface energy of low-index surfaces of stoichiometric α-Al_2O_3 and α-Cr_2O_3 ," Surf. Coat. Technol. **201**, 4205–4208.
Tolpygo, V. K. and Clarke, D. R. (**1999**). "Alumina scale failure resulting from stress relaxation," Surf. Coat. Technol. **120–121**, 1–7.
Veal, B. W. and Paulikas, A. P. (**2008**). "Growth strains and creep in thermally grown alumina: Oxide growth mechanisms," J. Appl. Phys. **104**, 093525.
Veal, B. W., Paulikas, A. P., and Hou, P. Y. (**2006**). "Tensile stress and creep in thermally grown oxide," Nat. Mater. **5**, 349–351.
Wang, C.-M., Thevuthasan, S., Gao, F., McCready, D. E., and Chambers, S. A. (**2002**). "The characteristics of interface misfit dislocations for epitaxial α-Fe_2O_3 on α-Al_2O_3 (0001)," Thin Solid Films **414**, 31–38.
Welzel, U. and Leoni, M. (**2002**). "Use of polycapillary X-ray lenses in the X-ray diffraction measurement of texture," J. Appl. Crystallogr. **35**, 196–206.
Wenk, H. R., Mathhies, S., Donovan, J., and Chateigner, D. (**1998**). "BEARTEX: A Windows based program system for quantitative texture analysis," J. Appl. Crystallogr. **31**, 262–269.